Tethering Forces of Secretory Granules Measured with Optical Tweezers

Vicente Valero, Thomas Nevian, Dominik Ho, and Manfred Lindau
School of Applied and Engineering Physics, Cornell University, Ithaca, New York 14853

ABSTRACT Fusion of a vesicle with its target membrane is preceded by tethering or docking. However, the physical mechanism of vesicle-tethering is unknown. To study this mechanism, we used eosinophil secretory granules, which undergo stimulated homotypic fusion events inside the cell during degranulation. Using a dual optical trap system, we observed tether formation between isolated eosinophil secretory granules. The results show that secretory granules interact stochastically with a target membrane forming physical tethers linking the vesicle and target membrane, rather than via interactions with the cytoskeleton. The necessary components are membrane-associated, and the addition of cytosolic components is not required. Tether-lifetime measurements as a function of applied mechanical force revealed at least three kinetically distinct tethered states. The tethered-state lifetimes of isolated eosinophil granules match the residence times of chromaffin granules at the plasma membrane in intact cells, suggesting that the tethering mechanisms reported here may represent the physiological mechanisms of vesicle-tethering in the cell.

INTRODUCTION

Vesicular transport entails a sequence of steps including vesicle formation, transport, tethering and docking, and eventually fusion. Although the fusion steps (in particular, exocytotic fusion pore openings) have been studied in great detail (1), there is little functional information available on tethering, the step that precedes vesicle fusion. Tethering and docking are terms describing the association of a vesicle with its target membrane. Tethering has been considered a link that extends over distances of more than 25 nm, whereas docking is thought of as a state where the vesicle and target membrane are held together within <5–10 nm (2). Thus, the term ''tethering'' refers to the initial interaction of a vesicle with its target membrane, whereas ''docking'' is widely thought to involve the trans-pairing of soluble *N*-ethymaleimide-sensitive factor attachment receptors (SNAREs) (3,4). Although a number of tethering factors were identified, it remains unclear what their molecular mechanism of vesicle tethering is, and which (if any) of these proteins and multisubunit complexes physically link a vesicle to its target membrane (5). In chromaffin cells, new vesicles approaching the membrane are docked or tethered (6), jittering as if they were in a small cage or as if attached to the plasma membrane via a tether ~70 nm long (7). This type of movement does not depend on intact SNAREs (8). It is unknown whether tethering involves a physical link between the membranes or else a cytoskeletal cage keeping the vesicle in place. Here we report on the first measurements, to our knowledge, of tethering forces between isolated horse eosinophil granules, using a dual optical trap.

MATERIALS AND METHODS

Cell preparation

Eosinophils were isolated from 125 mL of fresh blood from the jugular veins of horses (Equine Research Center, Cornell University, Ithaca, NY). During spontaneous sedimentation of red blood cells, the plasma, which contains leukocytes, was rapidly collected. The remaining erythrocytes were lysed by osmotic shock, and the final pellet was washed in Hanks' solution. To obtain 98% pure eosinophils, the solution was centrifuged over discontinuous Percoll (Biochrom, Berlin, Germany) gradients (9).

Granule isolation

To isolate granules, $\sim 5 \times 10^6$ purified horse eosinophils (Fig. 1 *a*) were suspended in 1 mL KCl-based buffer (125 mM KCl, 10 NaCl, 7 $MgCl_2$, 2 $CaCl_2$, 10 HEPES, and 5 EGTA) containing 140 nM free Ca^{2+} (calculated using WebMaxC, version 2.10, Stanford University, http://maxchelator.stanford.edu), protease inhibitors (pepstatin A, TPCK, aprotinin, leupeptin, and dithiothreitol, from Sigma, St. Louis, MO), and DNase I (grade II, Roche Boehringer, Indianapolis, IN), and disrupted by ~25 passages through a 25.5 syringe needle (Fig. 1 *b*). The suspension was then placed on top of a discontinuous Percoll gradient of 2 mL 79% Percoll at the bottom, overlaid with 1 mL 20% Percoll in a 15-mL Falcon tube, and centrifuged for 10 min at 500 rpm. The top 1 mL of buffer was removed, and the next 500 μL containing isolated granules, as well as small pieces from broken cells, were collected. The collected 500-μL suspension was gently mixed with 1 mL of KCl buffer and centrifuged at 500 rpm for 10 min in an Eppendorf centrifuge. We removed 1.2 mL of buffer from the top, leaving 300 μL of suspension at the bottom containing the granules. These 300 μL were then placed on top of 500 μL of fresh KCl buffer in an Eppendorf tube and centrifuged for 2 min at 500 rpm. The top 400 μL of buffer were discarded, leaving 400 μL of granule suspension. A sample chamber was filled with ~300 μL of an appropriately diluted solution containing granules at low concentration (~1 granule in 0.01 mm^2 of area) (Fig. 1 *c*). The chamber had a cover glass bottom, and was mounted on the stage of the inverted microscope (Axiovert 135 TV, Zeiss, Thornwood, NY).

Submitted March 3, 2008, and accepted for publication August 5, 2008.

Address reprint requests to Manfred Lindau, School of Applied and Engineering Physics, 212 Clark Hall, Cornell University, Ithaca, NY 14853. Tel.: 607-255-5264; Fax: 607-255-7658; E-mail: ml95@cornell.edu.

Thomas Nevian's present address is the Institute for Physiology, Bern University, Bühlplatz 5, CH-3012 Bern, Switzerland.

Dominik Ho's present address is the Dept. of Physics, Ludwig-Maximilians-University, Amalienstrasse 54, D-80799 Munich, Germany.

Editor: Joshua Zimmerberg.

© 2008 by the Biophysical Society
0006-3495/08/11/4972/07 $2.00

doi: 10.1529/biophysj.108.132670

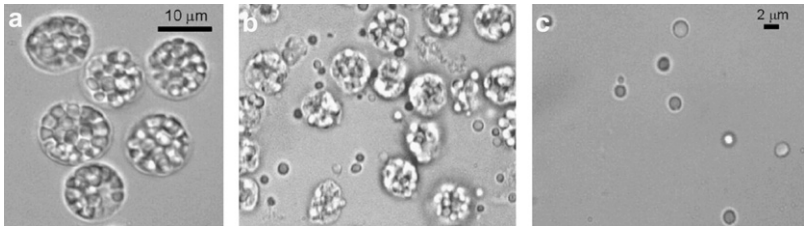

FIGURE 1 Horse eosinophil granule isolation. Purified horse eosinophils (*a*) were disrupted by passages through a syringe needle (*b*), and were purified (*c*) by Percoll centrifugation.

Dual optical trap setup

A dual optical trap was built, with one fixed and one steered trap. A diode-pumped neodymium-doped orthovanadate (Nd/YVO_4 infrared-laser emitting at 1064 nm, Millenia IR, Spectra-Physics, Mountain View, CA) was used as the light source for optical trapping. The beam was split by a polarizing beam-splitter. One beam was fixed in position, and the other was steered by a pair of acousto-optical deflectors (AODs) (see the Supplementary Material, Data S1, for details). A program was written in Visual Basic (Microsoft, Redmond, WA) to control the AODs and to acquire the video images. The program also controlled the piezo-electric translators for trap stiffness calibration.

Video imaging

Bright-field images of trapped granules were taken at 26–28 frames/second with a CCD video camera (SSC-M370, Sony, Niles, IL), using a digital video processor (DVP-32, InstruTECH, Great Neck, NY). With the objective used here (Zeiss Plan-Neofluar 100×13 Oil), pixels size corresponded to 97 nm/pixel in the object plane. Regions of interest of 60 × 100 pixels were saved for offline analysis.

Calibration of trap stiffness

For each granule in the fixed trap, trap stiffness was determined by experimental calibration, using a viscous-drag method. The optical trap held the vesicle 4–5 μm above the coverslip surface. Viscous drag forces were applied by moving a microscope substage with the sample chamber by 100 μm at different speeds, via attached piezo-electric translators (P-282, Physik Instrumente, Auburn, MA). The applied viscous-drag forces were estimated by applying Stokes' law $F = 6\pi\eta rv$, where η is the viscosity of the buffer, r is the radius of the vesicle, and v is the velocity of the flow. The granule was imaged while the substage was moved by 100 μm at various velocities, and displacement was determined as a function of applied force as calibration for the tethering experiment. This procedure was performed for each granule because trap stiffness may vary, depending on granule refractive index as well as laser power and focusing. The laser power was changed manually, using neutral density filters to modify trap stiffness.

The contour lines in Fig. 2, *b–d*, indicate the best fit of the displaced image of the resting granule (Fig. 2 *a*) (for details, see Calibration Image Analysis). Fig. 2 *e* shows the movement of the sample chamber (*black trace*) and granule displacement in the vertical direction (*red*, direction of viscous drag force) and horizontal direction (*blue*, perpendicular to viscous drag force). The position of the granule clearly follows the drag force. For a particular sweep, the downward displacement is rather constant, whereas the upward displacements show a slope (Fig. 2 *e*). This slope reflects a slope in velocity, and thus in applied force because of the hysteresis of the open-loop piezo movement (data not shown). For the quantitative analysis, only the linear parts (downward displacements) were used. The granule diameter was estimated as the distance between the intensity minima on each side of the granule image. The accuracy of this procedure was confirmed using polystyrene beads of known radius. Knowing the velocity of the chamber movement and the granule diameter, the viscous drag force can be estimated. Fig. 2 *f* shows that the displacement is proportional to the applied force, with a trap stiffness (inverse slope) of 25 pN/μm. For the range of granules used in our experiments (1.0–2.5-μm diameter), trap stiffness showed no systematic dependence on granule diameter (data not shown). Out of 111 granules, 74 (67%) had diameters between 1.3–1.8 μm, and the trap stiffness was 15–25 pN/μm. Using 2-μm-diameter polystyrene beads, the average trap stiffness using the same intensity was ~45 pN/μm, corresponding to their higher refractive index.

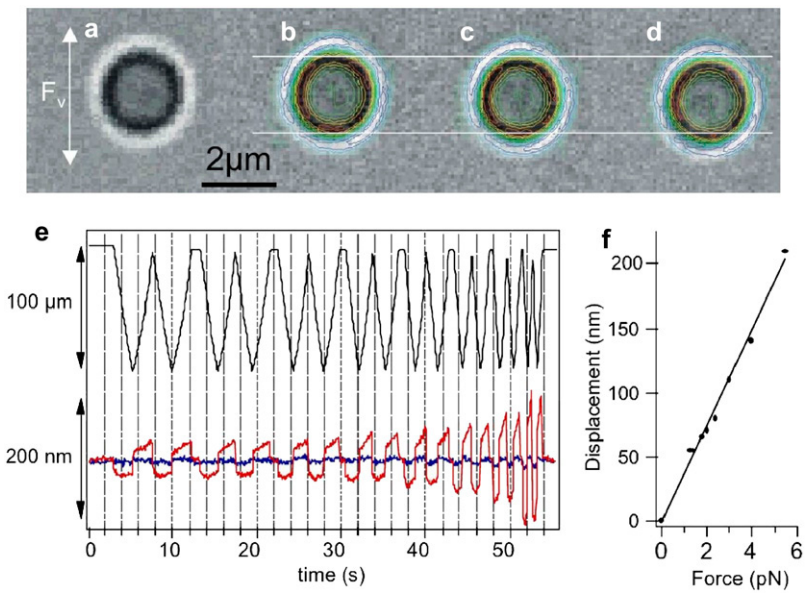

FIGURE 2 Calibration of trap stiffness for an individual granule by video-imaging of trapped granule. (*a*) Resting position in absence of friction force. (*b–d*) During movement of experimental chamber, the granule is displaced because of friction force F_v, depending on velocity of movement. To determine displacement, image (*a*) is used as a template (*contour lines*) to fit images of displaced granule (*b–d*). Horizontal white lines indicate position of granule at zero force. (*e*) Displacement of the microscope stage versus time (*black trace*) and displacement of granule in the direction of stage movement (*red*) and in the perpendicular direction (*blue*). Displacement of granule is proportional to viscous drag force (*f*), calculated from velocity v of stage movement $F = 6\eta rv$.

Calibration image analysis

When a viscous drag force was applied, the granule was displaced from its resting position. To characterize the displacement of a granule with high precision, a video image of the trapped granule was taken at its resting position, averaging ~10 acquired frames. To determine displacement while a force was applied, the image of the displaced granule was fitted using the image taken at resting position as a template. The fit parameters were the displacements Δx and Δy, an intensity scaling factor and a variable intensity offset to account for fluctuations in illumination. The image fitting was programmed in IGOR (WaveMetrics, Lake Oswego, OR), using only a selected region (typically, 40×40 pixels) containing the trapped granule. The initial guesses were updated from frame to frame, according to the fit result of the preceding frame. Moreover, the region of interest was updated and recentered according to the calculated displacement. To ensure that the algorithm did not provide values reflecting spurious local minima, some image sequences were fitted not only in the order in which they were acquired, but also in reverse order. The results showed stable positions, independent of sequence order. The automatic algorithm worked well when the frame-to-frame displacements were small. When the displacement of the granule from one frame to the next was too large, the granule was ''lost'' by the fit program, and new manual initial guesses had to be entered.

Measurement of tethering forces

To measure tethering forces, a granule was trapped with the fixed trap, and trap stiffness was calibrated. A second granule was subsequently trapped with the steered trap. The granules were then positioned at some distance and brought into contact for a defined time interval, using the automatic control program. The steered granule was moved in 15-nm steps by changing the frequency in the acoustic-optic deflector in 10-kHz increments. Granule-granule contact was indicated by observable movements of the granule in the fixed trap. After contact was observed, the direction of trap movement was reversed, pulling the steered granule back in 15-nm steps and 5-s or 20-s time intervals. The actual trap movement was performed at a speed of 90 nm/s. The determination of displacement of granules was similar to that for the calibration. However, the regions of interest were chosen such that the area of interest covered only ~70–80% of the image of the granule, excluding the part in contact with the second granule. This method ensured that the position determination for a granule was accurate, and was not disturbed by the presence of the second granule in the image. The measured displacement was converted to applied force, using the trap-stiffness calibration. All experiments were performed at room temperature (22–25°C).

RESULTS

Tethering forces between isolated secretory granules

Eosinophil granules perform homotypic granule-granule fusion events in the cell (9–12) to achieve high local concentrations of the released cytotoxic proteins by formation of degranulation sacs (13–15). Isolated horse eosinophil granules were used to determine if physical tethers are formed, linking their membranes. These granules have a high refractive index, and can be manipulated using a dual optical trap. A 1064-nm laser beam was split into two beams, with one beam fixed and the other steered by acousto-optical deflectors. The two granules shown in Fig. 3 *a* were trapped, with the left granule in the steered trap. The steered granule was then brought into contact with the granule in the fixed trap (Fig. 3 *b*), pushing it slightly to the right. When the steered granule was pulled back, the second granule was pulled to the left (Fig. 3 *c*), indicating that the granules were strongly tethered to each other.

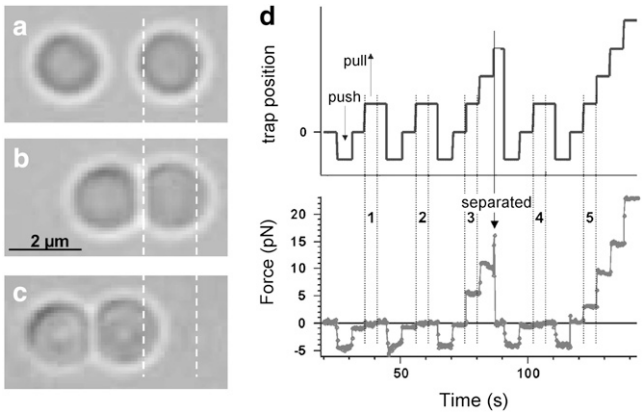

FIGURE 3 Granule-granule tether formation. (*a*) Right granule is held in stationary optical trap, and left granule in a steered optical trap. (*b*) Steered trap brings left granule in contact with right granule, pushing right granule slightly to right. (*c*) When steered trap pulls left granule back, right granule is pulled away from its resting position, indicating that a tether has been formed. Vertical dashed lines are provided to aid in identifying displacement of right granule. (*d*) Representative tethering force experiment. Steered optical trap was moved in steps of 25 nm (*top*) at 5-s intervals, and the force an the granule in the stationary trap is analyzed (*bottom*). Force on the granule in stationary trap is exerted by interaction with granule in steered trap. Numbers indicate pushing attempts to form a tether bond. Attempts 3 and 5 were successful. A tether dissociation event is indicated by arrow (*separated*).

To determine the applied force, the fixed trap stiffness was calibrated, applying a viscous drag force to the granule in the fixed trap (see Calibration of Trap Stiffness in Materials and Methods). A computer-controlled protocol was executed to move the granule in the steered trap stepwise at time intervals of 5 s or 20 s and increments of 15 nm, bringing it in contact with the granule in the fixed trap. After the contact time interval, the granule was pulled back, again at the same time intervals and increments as for the approach and contact. When a tether was formed, the granule in the fixed trap was pulled away from its resting position, following the steered granule. The applied forces were determined from measurements of the displacement of the granule in the stationary trap, using the trap stiffness from the calibration.

Fig. 3 *d* shows a representative experiment. The upper trace indicates the steered trap position, and the lower trace indicates the force applied to the granule in the fixed trap via its interaction with the granule in the steered trap. The first push and pull are indicated by arrows. Granules were pushed together with a force of ~4 pN. This trial, as well as the second trial, did not produce a tethered state, and no force was applied to the granule in the fixed trap when the steered granule was pulled back. The third trial, however, produced a tethered state, and the pull of the steered granule exerted a force of ~5 pN on the granule in the fixed trap. After 5 s, the steered granule was moved another step, and the force was increased to ~10 pN. When the steered granule was moved

again, the force increased again, but shortly afterward, the granules separated (*arrow* in Fig. 3 *d*), and the granule in the fixed trap moved back to its resting position. In the fourth trial, there was again no tethering. In the fifth trial, even larger forces could be applied to the tether, and a 23-pN force was applied for 5 s without separation. When the steered granule was moved farther, the granule in the fixed trap exceeded the escape force, and the experiment was terminated. Tethering forces could be analyzed in 81 of 111 experiments, giving a total of 368 force measurements. In the remaining 30 experiments, there was either no detectable tethering interaction, or the image quality was insufficient to fit the granule positions properly. Tether separations were observed for forces between 0.3 pN (no detectable tether formation) and 38 pN.

Force dependence of tether dissociation

The force dependence of tether-dissociation kinetics allows for a determination of tether-bond properties. For a simple bond, the dissociation rate constant k should depend on the applied force as

$$k = k_0 \exp\left(\frac{Fx}{k_B T}\right), \quad (1)$$

where k_0 is the rate constant at zero force, F the applied force, x the amount the bond needs to be stretched to reach the activation energy (energy landscape maximum), k_B the Boltzmann constant, and T the absolute temperature (16). To analyze the dependence of the dissociation rate constant on the applied force, we determined for each applied force the survival time of the tether. In Fig. 4 *a*, a pulling force of 7.7 pN was applied for 5 s without separation. Thus, the lifetime of this tether at this force was $\geq$5 s. The force was then increased in the next step to 13.2 pN. The lifetime of the tether at this larger force was 4.1 s, at which time the two granules separated. Survival curves were constructed, pooling the measured tether lifetimes in three groups of applied pulling force: 1–5 pN, 5–10 pN, and >10 pN. The average applied forces in these three pools were 2.4 pN, 6.7 pN, and 15.1 pN, respectively. Fig. 4, *b–d*, shows the survival curves for these three pools. A single exponential fit of the function

$$N(t) = N_D \exp(-kt) + N_S \quad (2)$$

of the low-force group (Fig. 4 *b*) gave a dissociation rate constant $k = 0.39 \pm 0.05\ s^{-1}$, with $N_D = 145 \pm 5$ and $N_S = 163 \pm 7$. The large value for the offset N_S represents a subset of ~50% of more strongly tethered vesicles that do not dissociate within a few seconds in this force range. For larger

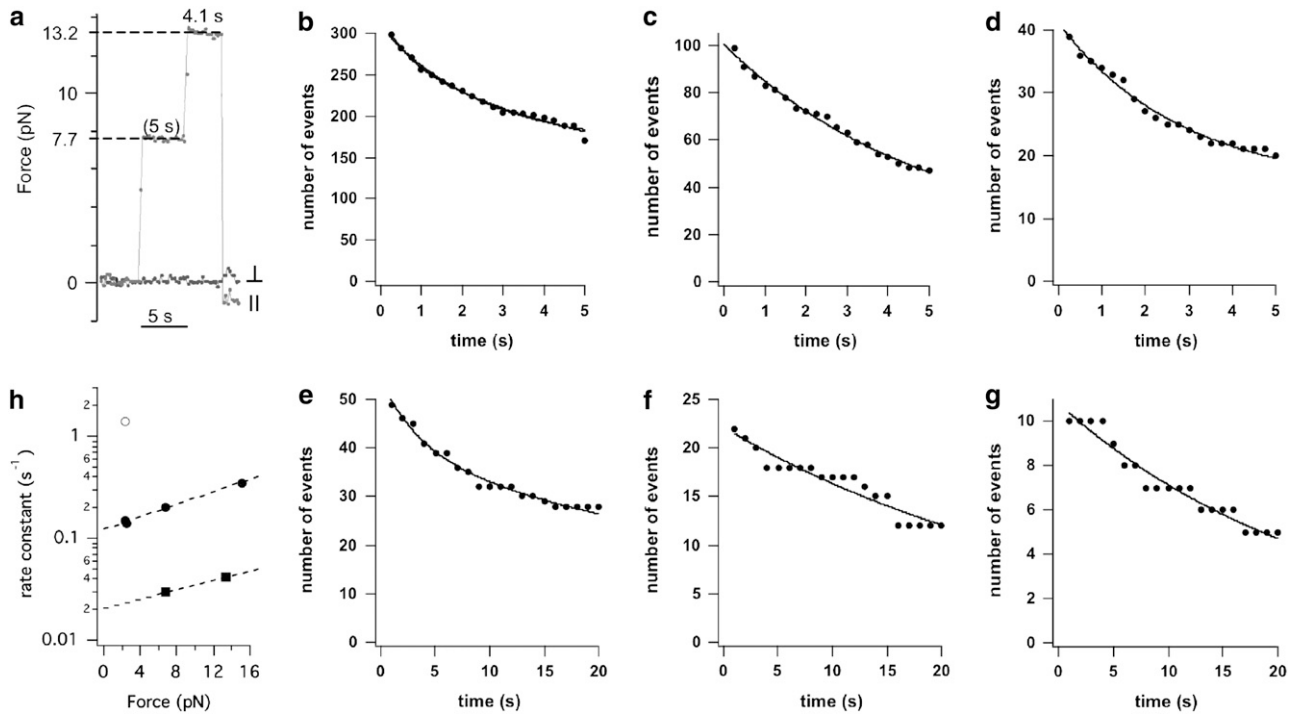

FIGURE 4 Kinetic analysis of tether disruption. (*a*) Trapped granule displacement converted to applied pulling force, exerted by steered tethered granule in direction of applied force (marked ||) and in perpendicular direction (marked ⊥). For each time interval, applied force was determined (*horizontal dashed lines*), and time was measured (as indicated) for which the granule remained tethered at this force. (*b–g*) Tether survival curves for 5-s time-interval protocol (*b–d*) and for 20-s time-interval protocol (*e–g*) in force groups, with mean values as indicated. Fitted curves are single exponential fits. (*b*) Double exponential fit is also superimposed (see text for fit details). (*h*) Force dependence of tether-dissociation rate constants (*open circle*, weak component, *solid circles*, intermediate main component, *solid squares*, strong component).

forces, a fraction of vesicles remained tethered at the end of the 5-s intervals. Combined exponential fits of these two groups indicate rate constants of $0.20 \pm 0.04\ s^{-1}$ and $0.35 \pm 0.05\ s^{-1}$ for the 5–10 pN and >10 pN groups, respectively, and a pool of ~15 more strongly tethered granules. This finding and the apparently rapid kinetics in the low-force group indicate heterogeneity in the tethering states, suggesting at least three distinct tethered states that dissociate at different forces and with different kinetics. The groups of Fig. 4, *c* and *d*, had mean applied forces of 6.7 pN and 15.1 pN, respectively. Substituting the corresponding average forces and rate constants in Eq. 1 provides a value for the length x by which the tethering bond needs to be stretched to reach the peak of the energy barrier

$$x = \frac{k_B T}{\Delta F} \ln\left[\frac{k(15.1pN)}{k(6.7pN)}\right] = 2.7\ \text{Å}.$$

This leads to an expected rate constant for the low-force $k(2.5\ \text{pN}) = 0.15\ s^{-1}$, which differs from the result of the single exponential fit. The rapid dissociation kinetics in the low-force group thus reflect disruption of a more loosely tethered state. The data in Fig. 4 *b* were therefore refitted, assuming a double exponential decay, with one rate constant fixed at $0.15\ s^{-1}$, the value expected for the more tightly tethered state. The result of this fit indicated that 53% of tethered granules dissociated with the $0.15\text{-}s^{-1}$ rate constant, 16% had a faster rate constant of $1.4\ s^{-1}$, indicating a weakly tethered state, and 31% were more strongly tethered (N_S). The data are thus consistent with at least three different tethered states where the kinetics of the intermediate state are described by the relation

$$k = k_0 \exp\left(\frac{Fx}{k_B T}\right), \quad \text{with} \quad k_0 \sim 0.13\ s^{-1} \quad \text{and} \quad x \sim 2.7\ \text{Å}.$$

To test if a dissociation rate constant of $\sim 0.15\ s^{-1}$ is indeed the main component in the 1–5-pN force group, the time intervals during which the vesicles were pushed together, as well as the time intervals to apply a particular pulling force to the tethers, were increased to 20 s. Kinetic data are shown in Fig. 4, *e–g*, for the same force groups as before. The average applied forces in the three groups were 2.5 pN, 6.6 pN, and 13.4 pN, respectively. A single exponential fit to the data in the 1–5-pN group (Fig. 4 *e*) yielded a rate constant $k = 0.14 \pm 0.01\ s^{-1}$, in excellent agreement with the expected main component in this force group from the data obtained with the 5-s interval. Thus, with this protocol, most of the tethers in this main group are dissociated in the low-force regime during the 20-s time interval. The data in Fig. 4, *f* and *g*, provide information on the more strongly tethered state. These data could be well-fitted, assuming an exponential decay to zero giving rate constants of $0.030 \pm 0.002\ s^{-1}$ and $0.042 \pm 0.002\ s^{-1}$ for the groups with 6.6 pN and 13.4 pN, respectively. For the tightly tethered state, this corresponds to values of $x = 2.0$ Å and $k_0 = 0.022\ s^{-1}$ in Eq. 1. The data strongly suggest at least three differently tethered states that dissociate with rate constants of $\sim 1.4\ s^{-1}$, $0.13\ s^{-1}$, and $0.024\ s^{-1}$ for low applied force (Fig. 4 *h*).

Elastic properties of tethered granules

In eight experiments, the same position-fitting algorithm that was used for the granule in the fixed trap could also be applied to the granule in the steered trap, to reveal a linear relationship between applied force and the change in the relative distance between the tethered granules (Fig. 5). Linear regression provided the slope or reciprocal ''spring constant'' of the tethered vesicles, which is $1/C_S = 13.2 \pm 1.3$ nm/pN. This spring constant presumably reflects the elastic properties of the tethers linking the granules, as well as the elastic properties of the granules themselves.

DISCUSSION

Tethering involves formation of physical links

Vesicular fusion is preceded by tethering of the vesicle to its target membrane (3,4), but it was unknown whether tethering involved physical links between the two membranes (5). The localization of chromaffin granules near the plasma membrane was studied extensively, and was found to be consistent with granules that were held at the plasma membrane by a tether ~70 nm long or by a molecular cage that would restrict granule motion in a similar way (7,8,17,18). We show here that isolated eosinophil granules form physical links when brought into contact with optical tweezers. All components required for the formation of strongly tethered states

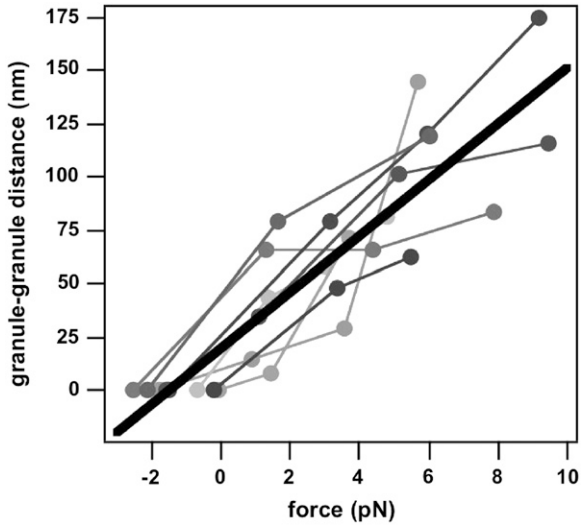

FIGURE 5 Force dependence of relative distance between two tethered granules. Measurements from same tether pair are connected by straight lines. Positions obtained when vesicles were slightly pushed against each other were arbitrarily taken as zero distance. Thick diagonal line is linear regression fit.

are retained on the membrane of the granules, and the addition of cytosol or cytosolic components is not required.

Horse eosinophil granules have a typical diameter of ~1.5 μm. Because of the small curvature, bringing them into contact creates a large contact area. When two spheres of radius r are brought into contact in the absence of applied force deforming the spheres, the radial distance s from the contact point to a point where the surfaces of the two spheres are separated by a distance $2d$ is $s = \sqrt{2rd - d^2}$. If we take $2d$ to be ~10 nm, a distance that should be close enough for membrane-protein interactions to occur, a value $s = 86$ nm is obtained for spheres with radius $r = 750$ nm. The corresponding estimate for the contact area would thus be ~0.023 μm^2. The elastic properties of tethered granules are characterized by a reciprocal spring constant of ~13 nm/pN (Fig. 5). When the two granules are pushed together by a typical force of 2–5 pN, we thus estimate that the distance between granule centers would be pushed together ~25–65 nm. The contact area where two membranes are within a 10-nm distance would then increase to ~0.08–0.17 μm^2. Even the contact area of 0.023 μm^2 in the absence of granule deformation would obviously be large enough to include a very large number of proteins, and many tether-forming proteins could be present within the contact area. However, as indicated in the experiment shown in Fig. 3, formation of tethers was actually not a very frequent event. It is, of course, possible that the frequency of tether formation was low because of missing cytosolic components, and that in the presence of such components, tether formation frequency would increase markedly.

Tether formation is presumably a consequence of molecular binding events between tethering components present in the two interacting membranes. Such binding events were stochastic in nature, and when granules were brought into contact, most trials failed to produce a tethering interaction. When granules were pushed together for ~5 s with a force of ~10 pN, only 33% of the trials led to tether formation. This stochastic behavior suggests that under the conditions of our experiments, there is a rather limited probability of forming a tether bond, and that the experiments reflect the properties of individual tethers rather than multiple tethers or nonspecific membrane interactions. It is, however, also possible that tethering components in the granule membrane are present in clusters that could form multiple tether bonds. Variability in the number of tether bonds formed may then give rise to kinetically distinct components.

Nevertheless, it appears likely that the tethering interactions are mediated by specific protein components associated with the membranes. The molecular identity of the specific components associated with or integral to the membranes that form the granule tethers and their regulation are still unknown. Further direct measurements of tethering forces, using biochemical and molecular manipulations, will be needed to demonstrate the physiological role of the granule tethering interaction described here. We anticipate that such experiments will provide much further insight into the molecular components and mechanisms of vesicle tethering.

Kinetics of tether dissociation

The tether dissociations show at least three kinetically distinct components with lifetimes of 0.7 s, 7.7 s, and 42 s at low force. Residence times of secretory granules at plasma membrane docking sites, recently determined in chromaffin cells using total internal reflection fluorescence microscopy (17), show three kinetically distinct states with similar lifetimes. The chromaffin granules arriving at the plasma membrane were grouped into three classes (visiting vesicles, with residence times <1 s; short-retained tethered, between 1–10 s; and long-retained tethered, >10 s). Our experiments suggest three states with tether lifetimes of 0.7 s, 7.7 s, and 42 s, which correspond well to the three states reported previously (17). The chromaffin granules with residence times <1 s were considered unrestrained (17). Our measurements indicate that tethering interactions with lifetimes <1 s involving physical links do occur, and raise the possibility that some of the visitor granules in chromaffin cells may actually form a tether with lifetimes <1 s. The good agreement of tether lifetimes observed for eosinophil granule interactions with the granule residence times at docking sites reported for intact chromaffin cells (17) suggests that the tethering interactions characterized here represent the properties of physiologically relevant tethers. They indicate that the mechanism keeping secretory granules in place at their target membrane involves physical links that are formed by membrane components, rather than mechanisms involving the cytoskeleton.

Biophysical properties of tethered granules

The force dependence of tether-dissociation kinetics yielded values of x at ~2.7 Å and ~2.0 Å by which tethering bonds must be stretched to reach the transition state for intermediate and strongly tethered states, respectively. The physical meaning of these values, however, should be interpreted with caution. The tether bond may very well not be a simple bond, but may have rather complex properties and, as discussed above, even the presence of multiple tether bonds cannot be excluded, in particular for the more tightly tethered states. Therefore, the values for x should be considered apparent x values.

The x values are remarkably close to those reported for single F_V-chain antibody binding (19). In contrast to the measurements of antibody-antigen interactions using atomic force microscopy (19), our experiments were performed using optical trapping, and involved elastic elements in the tether and/or granules such that tethered granules behaved as if connected via an elastic spring with spring constant $C_S = 0.076 \pm 0.008$ pN/nm. However, the forces applied to granules will nevertheless appear at the critical bond linking two granules. The similarity of x values obtained here with those obtained for antibody-antigen interactions may be taken as evidence that

our experiments reveal the properties of individual tether complexes. However, definitive proof for this hypothesis must await experiments with defined isolated tethering proteins.

The work W to stretch an elastic spring with spring constant C_S by distance l is $W = 1/2Fl = 1/2F^2/C_S$. The data in Fig. 3 include forces up to ~9 pN stretching the tether by ~120 nm, which corresponds to a mechanical work of $W \sim 5.3 \times 10^{-19}$ Nm or ~130 k_BT. However, only a small fraction of this work will actually stretch the tether bond. The kinetic analysis indicated that for the most tightly tethered state, the tether bond may be stretched by only ~2 Å to reach the peak of the activation energy. The largest force we applied to tethered granules was 38 pN, which reduced the activation energy for tether dissociation by 7.6×10^{-21} Nm, which is ~2 k_BT. Given the slow dissociation kinetics of the tightly tethered state, the activation energy is presumably much larger, indicating that in the experiments described here, the tether bond was stretched only slightly.

If a granule is tethered to its target membrane via an elastic element, thermal motion would be expected, depending on the stiffness of the elastic element, such as for particles in an optical trap. The mean-squared displacement $\langle \Delta s^2 \rangle$ of these fluctuations would thus be expected to be $\langle s^2 \rangle = k_BT/C_S$ or ~50 nm^2, corresponding to root mean-square position fluctuations of ~7 nm. Although this value is much smaller than the 70-nm tether length obtained from imaging the jittering motion of chromaffin granules at the plasma membrane in the *x/y* plane (7,8,17,18), it is rather close to the rapid jittering motion in the direction perpendicular to the plasma membrane, i.e., ~4 nm (18). It is thus possible that the rapid jittering motion of secretory granules perpendicular to the plasma membrane is attributable in part to the elastic properties of vesicle tethers.

SUPPLEMENTARY MATERIAL

To view all of the supplemental files associated with this article, visit www.biophysj.org.

We thank Carol Collyer, director of Equine Research Services (Cornell University), for supplying horse blood; Jonathan King and Joan Lenz for improvement of cell isolation; and Guillermo Alvarez de Toledo, Gregor Dernick, and Ismail Hafez for helpful discussions.

This work was supported by the Human Frontier Science Program (grant RG0227/98), the National Institutes of Health (grant R01 NS38200), the Nanobiotechnology Center (an STC program of NSF Agreement No. ECS-9876771), and the Secretaría de Estado de Universidades, Investigación, y Desarrollo of Spain.

REFERENCES

1. Lindau, M., and G. Alvarez de Toledo. 2003. The fusion pore. *Biochim. Biophys. Acta*. 1641:167–173.
2. Pfeffer, S. R. 1999. Transport-vesicle targeting: tethers before SNAREs. *Nat. Cell Biol.* 1:E17–E22.
3. Pfeffer, S. 2001. Vesicle tethering factors united. *Mol. Cell.* 8:729–730.
4. Cai, H., K. Reinisch, and S. Ferro-Novick. 2007. Coats, tethers, Rabs, and SNAREs work together to mediate the intracellular destination of a transport vesicle. *Dev. Cell.* 12:671–682.
5. Haas, A. K., and F. A. Barr. 2007. COP sets TRAPP for vesicles. *Dev. Cell.* 12:326–327.
6. Steyer, J. A., H. Horstmann, and W. Almers. 1997. Transport, docking and exocytosis of single secretory granules in live chromaffin cells. *Nature*. 388:474–478.
7. Steyer, J. A., and W. Almers. 1999. Tracking single secretory granules in live chromaffin cells by evanescent-field fluorescence microscopy. *Biophys. J.* 76:2262–2271.
8. Johns, L. M., E. S. Levitan, E. A. Shelden, R. W. Holz, and D. Axelrod. 2001. Restriction of secretory granule motion near the plasma membrane of chromaffin cells. *J. Cell Biol.* 153:177–190.
9. Scepek, S., and M. Lindau. 1993. Focal exocytosis by eosinophils: compound exocytosis and cumulative fusion. *EMBO J.* 12:1811–1817.
10. Hafez, I., A. Stolpe, and M. Lindau. 2003. Compound exocytosis and cumulative fusion in eosinophils. *J. Biol. Chem.* 278:44921–44928.
11. Hartmann, J., S. Scepek, I. Hafez, and M. Lindau. 2003. Differential regulation of exocytotic fusion and granule-granule fusion in eosinophils by Ca^{2+} and GTP analogs. *J. Biol. Chem.* 278:44929–44934.
12. Scepek, S., and M. Lindau. 1997. Exocytotic competence and intergranular fusion in cord blood-derived eosinophils during differentiation. *Blood*. 89:510–517.
13. Henderson, W. R., E. Y. Chi, A. Jörg, and S. J. Klebanoff. 1983. Horse eosinophil degranulation induced by the ionophore A23187: ultrastructure and role of phospholipase A_2. *Am. J. Pathol.* 111:341–349.
14. Tai, P.-C., and C. J. F. Spry. 1981. The mechanisms which produce vacuolated and degranulated eosinophils. *Br. J. Haematol.* 49:219–226.
15. Scepek, S., R. Moqbel, and M. Lindau. 1994. Compound exocytosis and cumulative degranulation by eosinophils and its role in parasite killing. *Parasitol. Today.* 10:276–278.
16. Bell, G. I. 1978. Models for the specific adhesion of cells to cells. *Science*. 200:618–627.
17. Toonen, R. F., O. Kochubey, H. de Wit, A. Gulyas-Kovacs, B. Konijnenburg, J. B. Sorensen, J. Klingauf, and M. Verhage. 2006. Dissecting docking and tethering of secretory vesicles at the target membrane. *EMBO J.* 25:3725–3737.
18. Allersma, M. W., M. A. Bittner, D. Axelrod, and R. W. Holz. 2006. Motion matters: secretory granule motion adjacent to the plasma membrane and exocytosis. *Mol. Biol. Cell.* 17:2424–2438.
19. Schwesinger, F., R. Ros, T. Strunz, D. Anselmetti, H. J. Guntherodt, A. Honegger, L. Jermutus, L. Tiefenauer, and A. Pluckthun. 2000. Unbinding forces of single antibody-antigen complexes correlate with their thermal dissociation rates. *Proc. Natl. Acad. Sci. USA*. 97:9972–9977.